AIAA JOURNAL
Vol. 48, No. 7, July 2010

Numerical Investigation on the Aerodynamics of Oscillating Airfoils with Deployable Gurney Flaps

Michael P. Kinzel* and Mark D. Maughmer†
Pennsylvania State University, University Park, Pennsylvania 16802
and
Earl P. N. Duque‡
Intelligent Light, Rutherford, New Jersey 07070

DOI: 10.2514/1.J050070

To assess their application to rotorcraft, the two-dimensional aerodynamics of deployable Gurney flaps, referred to as miniature trailing-edge effectors, are explored using computational fluid dynamics. These deployable devices have a height of only a few percent of the airfoil chord and deploy normal to the airfoil surface near the trailing edge. Their small size, low inertia, and small added mass make them well suited for deployment in high-frequency applications such as those needed for rotorcraft. A combination of wind-tunnel measurements using airfoils fitted with Gurney flaps and unsteady circulatory theory are used to validate the computational fluid dynamics, and grid and time-resolution studies are used for code verification. Qualitative and quantitative agreement of the effects of a Gurney flap with experiments and theory suggest that the computational fluid dynamics results are valid. These investigations examine the effects of the chordwise positioning and deployment frequency of the miniature trailing-edge effectors. In doing so, their operation on both static and dynamically pitching airfoils is considered. Through these studies, a number of physical insights into miniature trailing-edge effectors and Gurney flap aerodynamics have been obtained. These insights have led to the introduction of a scaling parameter that easily accounts for compressibility effects, an understanding of the aerodynamic consequences due to positioning miniature trailing-edge effectors upstream of the trailing edge, and an assessment on the benefits of using of miniature trailing-edge effectors for active stall alleviation on an airfoil oscillating in pitch.

Nomenclature

Symbols

c	=	airfoil chord
c_d	=	profile-drag coefficient
c_l	=	section lift coefficient
c_m	=	section pitching-moment coefficient about the quarter-chord point
k	=	reduced frequency, $\omega c/2V$
M	=	Mach number
R	=	Reynolds number based on freestream conditions and airfoil chord
V	=	freestream velocity
x	=	airfoil abscissa
α	=	angle of attack relative to x axis, deg
α'	=	scaled angle of attack, $(\alpha - \alpha_{-n\text{STALL}})/(\alpha_{p\text{STALL}} - \alpha_{-n\text{STALL}})$
δ	=	miniature trailing-edge effector deflection height from airfoil surface
Δc_l	=	Gurney flap effect to the section lift coefficient
Δc_d	=	Gurney flap effect to the section drag coefficient
Φ	=	phase angle between lift and miniature trailing-edge effector position, deg
ω	=	angular flap deployment frequency, rad/s

Subscripts

max	=	maximum
∞	=	reference to the freestream value
pSTALL	=	reference to positive stall
nSTALL	=	reference to negative stall

Received 15 July 2009; revision received 4 February 2010; accepted for publication 20 February 2010.

*Research Associate, Applied Research Laboratory. Member AIAA.
†Professor, Department of Aerospace Engineering. Associate Fellow AIAA.
‡Manager of Applied Research. Senior Member AIAA.

I. Introduction

THE aerodynamics of miniature trailing-edge effectors, devices based on Gurney flaps, are explored with regard to their application to rotorcraft. A Gurney flap is an aerodynamic device having a height of between 1 and 5% of the airfoil chord and mounted normal to the airfoil surface near the trailing edge [1]. Compared with a baseline airfoil, the maximum lift coefficient has been shown to increase up to 30% using a Gurney flap having a height of only 2% chord [2]. A miniature trailing-edge effector, or MITE, extends the concept of a Gurney flap by being deployable.

As with Gurney flaps, the effectiveness of a MITE depends on its height relative to the local boundary-layer thickness [3]. This is the cause of certain limitations of Gurney flaps and MITEs, such as a diminishing effect as the airfoil approaches negative stall when positioned on the lower surface of a wing. Alternatively, this suggests that an upper-surface device will display little or no effect to the aerodynamics of an airfoil stalling at positive angles of attack, as experimentally verified in [2]. In other words, these devices are too small to affect the separated flow of a stalled airfoil unless moved ahead of the separation point [4].

MITEs are a recent innovation and have yet only been considered for a small number of applications. One of these is directed toward the control of tailless aircraft such as the Boeing blended-wing-body aircraft [5], while another deals with fixed-wing aircraft flutter control [6–9]. In both cases, MITEs show great promise in that they can provide aerodynamic effects similar to plain flaps but have the benefit of low inertia and power requirements, making them ideal for high-frequency deployments. Other studies have explored the use of MITEs as a low-power and highly controllable means of load alleviation on both wind turbines and helicopters, where the devices are expected to mitigate high-loading events to prevent blade failure [4,10–13]. For helicopter applications, the use of Gurney flaps on rotor blades with the intention of increasing high-speed flight performance was first considered by Kentfield [14]. While this study

did not examine in detail the penalties due to increased drag and nose-down pitching moment, the impact of these issues has been explored more recently in some detail by Yee et al. [15]. In another study, Gurney flaps have been investigated for dynamic-stall alleviation when used in conjunction with a drooped leading edge [16,17].

For the application considered here, that of rotorcraft performance enhancement and vibration control, it is anticipated that MITEs would be segmented along the trailing edge of helicopter rotor blades and deployed azimuthally as required [18–22]. They can be placed upstream of the trailing edge to allow them to be stowed within the airfoil where there is sufficient thickness to accommodate them along with any required deployment mechanisms. This allows them to deploy normal to the surface, rather than pivot, which helps to minimize actuation loads. Their anticipated uses are to enhance rotor performance by being deployed and retracted during one rotor revolution to achieve desired radial and azimuthal lift distributions, and/or in higher frequency deployments to mitigate vibration and noise. As a result of their inertia and required actuator loads being significantly less than those required by the more conventional methods being considered, such as trailing-edge flaps, MITEs represent an alternative that warrants additional consideration.

To aid in the understanding of Gurney flaps and MITEs for the various proposed applications, a number of computational studies have been presented in the recent literature. Many of the initial studies were performed on MITEs used for flutter suppression. In one such study, an analysis of MITEs on a NACA 0012 airfoil was performed using computational fluid dynamics (CFD) [8,9]. In this study, it was found that the desired aerodynamic benefits of MITEs are present at high-frequency deployment rates and are closely associated with the aerodynamics predicted by Theodorsen's circulation function [23]. Unsteady particle image velocimetry of these MITE-like devices, which pivot rather than deploy in a knife-edge sense [24], display a flow structure that is dominated by counter-rotating vortices forming behind the flap similar to that observed for a Gurney flap [1]. Upstream MITEs, located so that they can be stored within the airfoil [10], were first investigated in the frequency domain for the VR-12 and S903 airfoils using CFD in [19,20]. As will be considered further here, it was found that the aerodynamics deviated from Theodorsen's theory due to vortex-induced loading on the airfoil downstream of the flap. Similar investigations on upstream microtabs have been performed in the time domain and a very similar vortex-induced loading is predicted [12,13]. One other combined CFD/experimental investigation has been performed on upstream MITEs [25]; however, the wind-tunnel model used only employed a single pressure orifice on each surface downstream of $x/c = 0.6$. Given the extreme pressure variations that occur over the aft part of the airfoil in both steady (Gurney flap) and unsteady (MITE) cases, these results are less than ideal for validation purposes.

The development of analytical models to account for the unsteady aerodynamics of MITEs has also been undertaken in several studies. The first such models were developed for trailing-edge fitted MITEs used a modified Theodorsen theory as a starting point for providing unsteady loads for flutter suppression [9]. A similar model was developed for compressible flows [19,21], valid for rotorcraft performance analyses, by adapting the Hariharan–Leishman unsteady-flapped airfoil model [26], which was more recently adapted to predict the behavior of upstream MITEs [22].

To study the potential of MITEs for the proposed rotorcraft applications, the aerodynamics of the devices are explored at various chordwise locations, deployment frequencies, and Mach numbers. Special attention is given to the use of MITEs for stall alleviation and increasing $c_{l,\max}$. Static and oscillating Gurney flap-equipped airfoil wind-tunnel measurements, along with grid resolution studies, are used to lend confidence that the CFD predictions are valid. Comparisons with the classical theory of Theodorsen are used to validate the unsteady predictions [23]. Once this has been done, the CFD predictions are used to develop an understanding of MITE deployment aerodynamics and facilitate the generation of design-level unsteady aerodynamic models that can be used to explore the potential of MITEs for improving rotorcraft performance. Finally, these analyses have additional utility in that experiments can be designed with the benefit of a priori knowledge of the anticipated aerodynamic behavior. For example, the data acquisition process that is used needs to consider the strong, vortex-induced pressure gradients and fluctuations near the MITEs as predicted by CFD. Without such guidance, it is likely that experiments will miss some of the important aspects of the unsteady aerodynamics.

The CFD assessments of MITEs as applied to rotorcraft presented herein are based on extensions of validated and verified CFD models of clean and Gurney-flapped airfoils. The verification uses grid and temporal resolution studies for a Gurney-flapped airfoil and dynamic MITEs. The validation initiates with load prediction comparisons of static clean and Gurney-flapped airfoils between CFD results and those obtained using a combination of wind-tunnel experiments and airfoil analysis codes. These comparisons demonstrate that the CFD methods predict the aerodynamics reasonably well, especially in terms of the magnitudes of the aerodynamic changes due to Gurney flaps. Next, dynamic simulations are validated using: 1) comparisons of load predictions and measurements from wind-tunnel experiments for clean and Gurney-flapped airfoils in dynamic stall, and 2) comparisons of theoretical and numerically predicted loads for an airfoil with oscillating lift due to oscillatory MITE deployments. The ability to capture agreeable unsteady aerodynamics, dynamic-stall trends, and, more importantly, the aerodynamic changes due to Gurney flaps, gives confidence in these CFD predictions of MITE aerodynamics. The unsteady aerodynamic analyses of active MITEs yields insights on the effects of deployment frequency and freestream conditions, and enables preliminary assessments of their potential to actively increase $c_{l,\max}$ on oscillating airfoils that are representative of rotorcraft applications. Although the lack of experimental validation data for MITEs limits the certainty of the results, validation and verification of the individual components of the MITE deployment scenario gives confidence in the assessments.

II. Computational Methods

Although the Navier–Stokes solver OVERFLOW2 [27,28] is used for the detailed analyses of Gurney flaps and MITEs, other airfoil design and analysis codes are used for validation purposes. These include the subsonic, compressible, steady, Euler/integral boundary-layer code MSES [29], and the incompressible vortex-panel/integral boundary-layer code XFOIL [30]. These methods provide fast and reliable predictions for the steady-flow aerodynamics over airfoils and are used to validate OVERFLOW2 predictions when no wind-tunnel data is available. For these XFOIL and MSES results, transition is fixed at $0.05c$ on the upper surface and $0.1c$ on the lower surface. The transition parameter NCRIT is set to 9.0 [29,30].

A. Description of the CFD Solver

The CFD code OVERFLOW2 is used for the analyses of airfoils employing Gurney flaps or MITEs. OVERFLOW2 is a Reynolds-averaged Navier–Stokes (RANS) solver that uses structured overset grids, which allow for relative motion between bodies [27,28]. In an overset grid methodology, the grid boundaries are interpolated from neighboring grids. Thus, the grids can be attached to specific components without the requirement that they match faces or vertices. In this case the moving bodies are the airfoil and the MITE. All of the simulations presented herein use the Spalart–Allmaras one-equation turbulence model with no transition point specified [31]. Thus, the walls are treated using a model that resembles a condition that is fully turbulent. This turbulence model is standard for aerodynamic flows and generally performs well for attached flow conditions; however, massive separation often requires three-dimensional, eddy-resolving approaches. These cases also use double precision arithmetic, second-order accurate central differencing in space and time, and a first-order accurate implicit-Euler scheme. Steady solutions are obtained after the forces have converged and display residuals of machine precision. Unsteady solutions are achieved using several unsteady cycles after the observed statistics in the force history have stabilized.

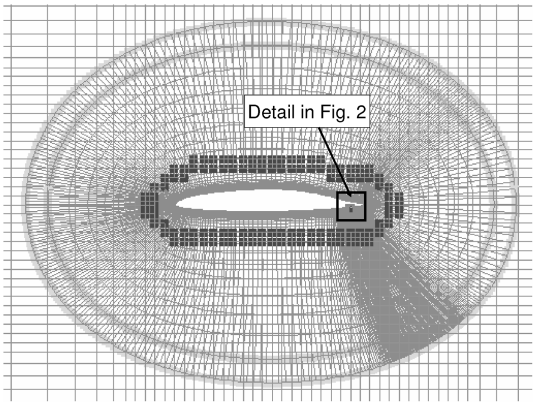

Fig. 1 General grid scheme, boxgrid, and airfoil O-grid.

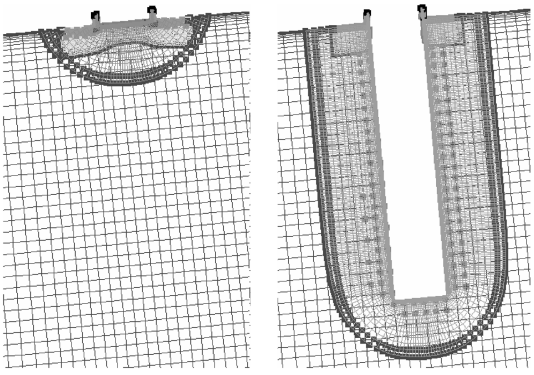

a) **b)**

Fig. 2 Detail of the Gurney-flap-airfoil junction: a) baseline model, and b) Gurney-flap model.

B. Grid Generation

The general grid scheme used is displayed in Figs. 1 and 2. A boxgrid is used to extend the domain from the airfoil to the far-field boundaries approximately 10 chord lengths from the airfoil surface. The airfoil is composed of two O-grids, one having dimensions of 366×78 extending $0.3c$ from the airfoil surface (Fig. 1), and the other having dimensions of 163×25 and extending $0.003c$ from the surface of the Gurney flap (Fig. 2). All of the grids were created using Chimera Grid Tools [32] and generated using the best overset practices [33]; however, additional refinements are made through the depth of the flap and in the region near the MITE. With the exception of the near-wall cells used to resolve the boundary layer, the airfoil grid uses a constant spacing throughout the depth of the flap to provide consistent spatial discretization throughout the full deployment of the MITE. The mean, nearly isotropic cell size in this region is roughly $\Delta x = \Delta y = 0.0004c$. At the Gurney flap/airfoil junction, some orphan points exist. Orphan points occur where the points are either donorless or have insufficient overlap. In this case these points are buried within the airfoil to prevent them from affecting the solution in the outer-flow and boundary-layer regions.

1. *Grid Refinement Study for Gurney Flaps*

To ensure that discretization errors are small, several grids with variations in refinement have been investigated for a Gurney-flap-equipped airfoil at an angle of attack of zero. To minimize the effect of orphan points in the grid refinement study, a consistent grid is used in the area where they occur, that is, near the Gurney-flap/airfoil junction. Spatial refinements are made in both directions on both the airfoil O-grid and the far-field grid. These investigations are based on the time-averaged forces for an unsteady, static Gurney-flap simulation. Force and moment coefficient predictions for the case where the Gurney flap is positioned at the trailing edge are given in Table 1, along with the dimensions of the corresponding O-grid used in obtaining the given solution. For this case the time-averaged forces and moments show convergence toward the finest grid size considered. The general grid size used throughout is similar to the medium case, which should yield lift, drag, and pitching moments within 2% of the finest grid. A similar study was performed when the MITE was positioned upstream of the trailing edge, at $x/c = 0.9$, the results of which are summarized in Table 2. In this case, the predicted coefficients display a slight increase in sensitivity to the medium resolution; however, the predicted loads display little variation between the medium- and fion Thursdayne-resolution meshes. It should be noted that for both Gurney-flap positions, the coarse mesh does not sufficiently resolve the vortex-street development downstream of the flap, and that a high-resolution mesh in that region appears to be important for capturing the unsteady features.

Table 1 Spatial refinement for a Gurney flap positioned at the airfoil trailing edge

	Grid size	c_l	c_d	c_m
Coarse	162×45	0.39639	0.01515	−0.06462
Medium	322×85	0.46690	0.01693	−0.06982
Fine	643×169	0.46424	0.01666	−0.06998

Table 2 Spatial refinement for a Gurney flap positioned at 0.9*c* from the airfoil leading edge

	Grid size	c_l	c_d	c_m
Coarse	195×41	0.61492	0.02923	−0.08590
Medium	338×80	0.52672	0.03066	−0.07328
Fine	775×159	0.51088	0.03128	−0.07218

2. *Temporal Refinement Study for Gurney Flaps*

The sensitivity to the time-step size was investigated to ensure that a sufficient temporal resolution is used to predict the unsteady flow structure and aerodynamics of a Gurney-flap-equipped airfoil. Again, in these models orphan points exist, which tend to decrease the stability of the numerical scheme. Thus, to achieve a stable, integrated solution, a relatively small time step is required. The time-step sizes used throughout these studies, in nondimensional time $t^* = tV/c$ range from 5.0×10^{-4} to 1.25×10^{-3}. Investigations of the predicted unsteady forces of a Gurney-flap-equipped airfoil for $R = 4.0 \times 10^6$ suggest that this size range of time step accurately predicts the mean values and amplitudes. Although the predicted shedding frequency displays differences of up to 20%, this does not affect the forces and moments of interest, provided that the shedding frequency is higher than the deployment frequency, as is the case here.

3. *Mesh and Temporal Refinement Studies for Unsteady MITE Simulations*

The effects of various computational mesh and temporal resolutions for dynamic MITE simulations have also been explored. From these investigations, the mesh density was only varied in the regions ahead, aft, and through the depth of the MITE. The cell sizes in these regions maintained a roughly rectangular size with $\Delta x/c = 0.0008$, 0.0004, and 0.0002 for the coarse, medium, and fine meshes, respectively. The results for the lift and drag coefficients are displayed in Fig. 3. These studies were performed with $k = 1.0$, $R = 4.0 \times 10^6$, and $M = 0.4$. Here, the dynamics that correspond to the lift coefficient appear to be well resolved for the medium and fine meshes, and although the plot is omitted, the pitching-moment coefficient convergence resembles that of the lift. Likewise, the drag coefficient is well predicted for all grid resolutions. Throughout these studies, a rectangular grid spacing of $0.0004c$ in the vicinity of the MITE is used. Time-step sizes through dynamic simulations were also examined and, as can be observed in Fig. 3, halving the time-step size has no discernable effect on the solution.

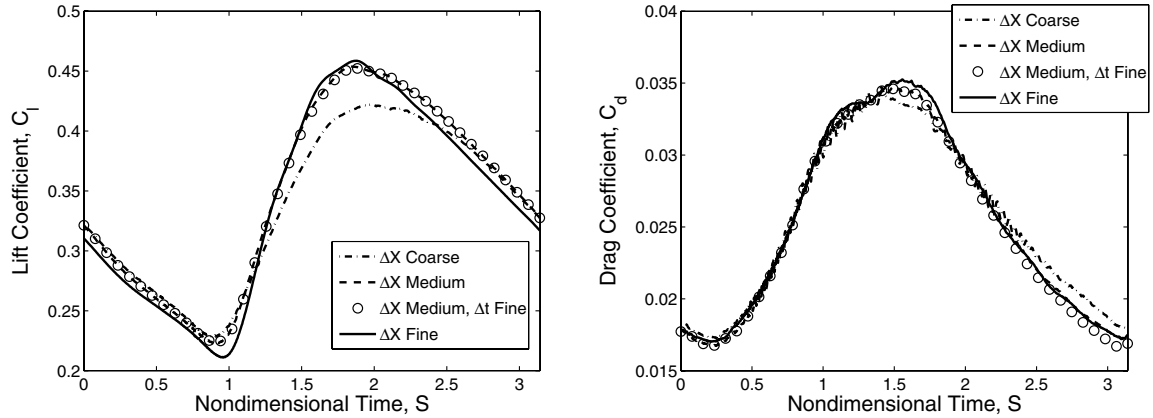

Fig. 3 Effect of grid resolution and time-step size on the predicted lift and drag coefficients for a deploying MITE.

III. CFD Validation for Static Conditions

A. Validation at Low-Speed Operating Conditions

Of the Gurney-flap configurations employed on the S903 airfoil and used in experiments performed in the Pennsylvania State University low-speed, low-turbulence wind tunnel [2], three were modeled in OVERFLOW2. These include the baseline S903 airfoil (S903-BL), the S903 airfoil with a Gurney-flap height of $0.01c$ mounted at the airfoil trailing edge (S903-1-100), and the S903 airfoil having a Gurney-flap height of $0.02c$ positioned $0.9c$ from the leading edge (S903-2-90). For consistency with dynamic MITE simulations, the baseline airfoil is modeled with the Gurney flap retracted to the flush position as shown in Fig. 2a.

The aerodynamic characteristics for the baseline airfoil, obtained from experiment and predicted using OVERFLOW2, MSES, and XFOIL, are presented for comparison in Fig. 4. The experimental results were obtained with transition fixed at $0.02c$ on the upper surface and $0.07c$ on the lower. It is observed that OVERFLOW2 predicts the aerodynamic characteristics reasonably well, although the lift coefficient deviates slightly from the experimental results and those of MSES and XFOIL at angles of attack approaching stall. Improved agreement with the experimental results near stall are achieved in OVERFLOW2 using $M = 0.3$, rather than the actual $M = 0.1$, which introduces little or no compressibility effects but improves accuracy and convergence. MSES and XFOIL calculations agree well with the experimental results, although MSES was unable to converge to steady solutions near stall for this airfoil.

A comparison of the aerodynamic characteristics predicted by OVERFLOW2 and those obtained experimentally for the S903-BL, S903-1-100, and the S903-2-90 airfoil configurations are presented in Fig. 5. It should be noted that the S903-2-90 measurements were obtained with a naturally occurring transition, while the CFD predictions were run as fully turbulent. This particular airfoil, however, was designed for the lift coefficient to be insensitive to the transition location, as is experimentally verified in [2], such that the lift coefficient predictions expected to be insensitive to the transition location. The lift curves, and their slopes, continue to agree well with experiment through the linear range, and the drag coefficient is predicted well near $c_l = 0$, although the agreement becomes progressively worse as the angle of attack increases. The effect of the Gurney flap is modeled correctly through stall, and the necessity of modeling the laminar flow regions seems to be relatively unimportant here for capturing the mean aerodynamic effects of the Gurney flap.

The predicted flowfield in the vicinity of the Gurney flap, using the streamlines of time-averaged solutions, is presented in Fig. 6. The predicted flow structure when the Gurney flap is mounted at the trailing edge, or the S903-1-100 case, is presented in Fig. 6b. This flow structure is highly similar to that predicted by Liebeck [1], shown in Fig. 6a, measurements observed using laser Doppler anemometry measurements [34], and recent particle image velocimetry and dye-injection studies [35]. For the upstream Gurney-flap location, the predicted flowfield for the S903-2-90 case, presented in Fig. 6c, is also reasonable and consistent with experimental results, including capturing the vortex structure [35] and the accompanying low-pressure region present downstream of the flap [2].

B. Validation for High-Speed Operating Conditions

For helicopter rotors, the performance of MITEs at various Mach numbers is important. Transonic experiments [36] and CFD results [37] have shown that the behavior of Gurney flaps in transonic flows are similar to that observed at low speeds. The authors are unaware of any investigations of Gurney flaps over the wide range of Mach numbers and operating conditions experienced by a helicopter rotor airfoil. Thus, the VR-12 and VR-15 airfoils [38] having Gurney flaps

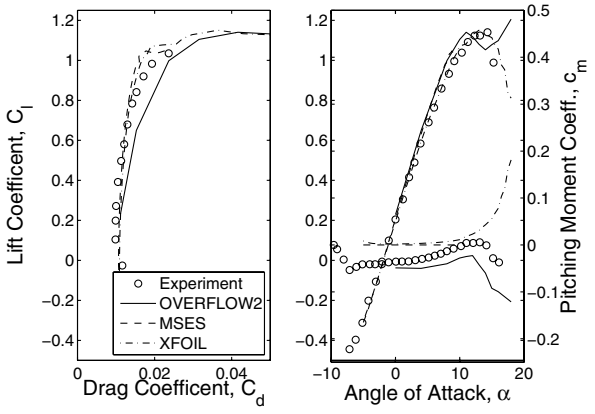

Fig. 4 Comparison of the aerodynamic characteristics determined with OVERFLOW2, MSES, XFOIL, and experiment [2] (PSU-EXP) for the baseline S903 airfoil ($M = 0.1$, $R = 1.0 \times 10^6$).

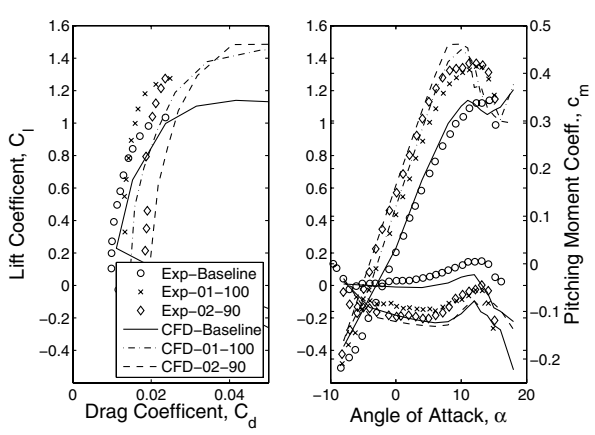

Fig. 5 Comparison of CFD (lines) and experimental (symbols) results for various Gurney-flap geometries ($M = 0.1$, $R = 1.0 \times 10^6$).

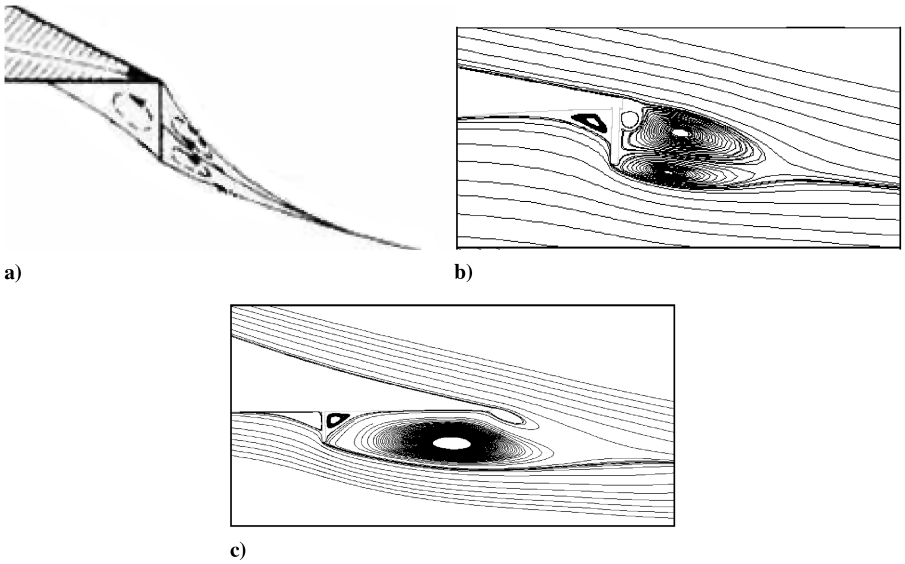

Fig. 6 Time-averaged solution streamlines: a) Liebeck's hypothesized flow structure [1], b) S903-1-100, and c) S903-2-90.

have been investigated over the appropriate range of operating conditions. As no experimental data is available, the baseline airfoils are validated against MSES and XFOIL to gauge the accuracy of the OVERFLOW2 results. All simulations are obtained over a range of Mach numbers, with a constant $R = 4.0 \times 10^6$. For brevity, only results for the VR-12 airfoil are presented, although those for the VR-15 are presented in [19].

1. *Baseline VR-12 Airfoil*

Before looking at the changes in the aerodynamic characteristics due to a Gurney flap, the baseline characteristics of the VR-12 were predicted for $M = 0.2$, 0.45, and 0.6. The results are shown in Fig. 7, although the $M = 0.45$ case is omitted for clarity. In examining the $M = 0.2$ case, it should be noted that the lift coefficients predicted by OVERFLOW2 agree well with those of XFOIL and MSES, except that MSES predicts a slightly higher maximum lift coefficient than does OVERFLOW2 and XFOIL. While none of these codes are considered to be reliable for predicting $c_{l,\max}$, at least using the methods applied within these studies, they all do agree to some extent. At higher angles of attack, OVERFLOW2 predicts higher drag coefficients than both MSES and XFOIL, while the pitching-moment coefficients predicted by OVERFLOW2 are nearly the mean of those predicted by MSES and XFOIL. At increased Mach numbers, the lift, drag, and pitching-moment coefficients predicted by OVERFLOW2 continue to agree with MSES through stall. XFOIL results are not included at the higher Mach numbers, as it is an incompressible code.

Overall, the OVERFLOW2 lift and moment coefficient predictions for this airfoil are in good agreement with those of MSES and, at the lower Mach numbers, XFOIL. The drag coefficient predictions, however, are consistently higher than those of MSES and XFOIL for the low Mach numbers, especially at angles of attack away from stall. This is likely an effect of inaccuracies that occur when using a nonpreconditioned, compressible solver at low Mach numbers. In the context of the proposed rotorcraft applications, however, where the focus is largely on MITE deployments for retreating blade stall mitigation, achieving the correct lift-curve and near-stall drag is of much greater importance than being able to accurately predict the drag at lower angles of attack.

2. *Gurney-Flapped VR-12 Airfoil*

Now, having some understanding of the validity of the computational results, the aerodynamic behavior of airfoils equipped with Gurney flaps was computed. In particular, predictions were made to explore the effects of compressibility on a VR-12 airfoil having a Gurney flap of $0.01c$ in height located at the trailing edge. The predicted aerodynamic characteristics for the Gurney-flap-equipped airfoil obtained for $M = 0.2$ and 0.6 are compared with those of the baseline in Fig. 8. The predicted aerodynamics with compressibility effects are as expected, and consistent with those of other investigations of Gurney flaps in both incompressible and compressible flows [3,4,17,34,37]. Further, the calculated changes to the lift, drag, and pitching-moment coefficients are plotted against a scaled angle of attack, referred to as α', in Fig. 9. This scaling normalizes the results based on the positive and negative stalling angles of attack of the baseline airfoil, such that 0.0 represents the angle of attack where it reaches negative stall and 1.0 represents the angle of positive stall. This normalized angle of attack is given by

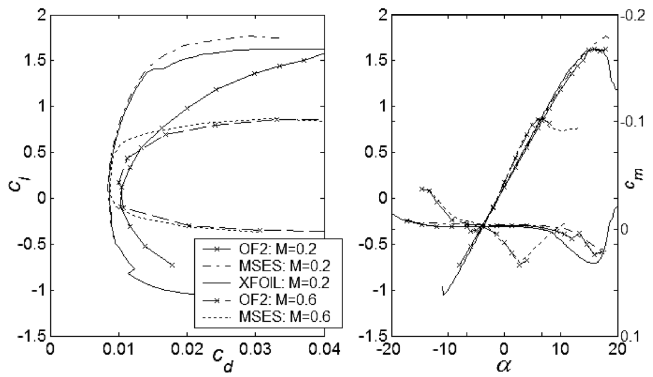

Fig. 7 Comparison of OVERFLOW2 (OF2), XFOIL, and MSES predictions of the baseline VR-12 airfoil for $M = 0.2$ and 0.6 and $R = 4.0 \times 10^6$.

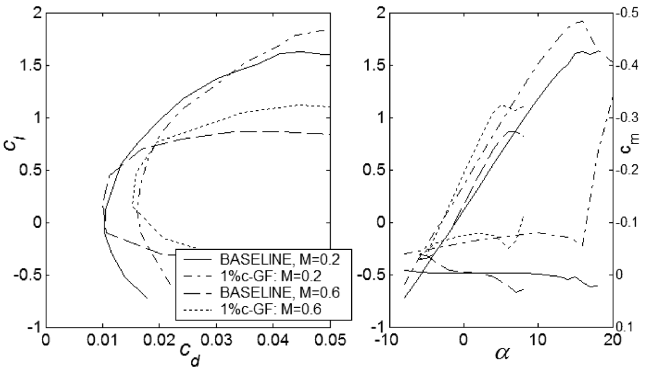

Fig. 8 OVERFLOW2 predictions of the VR-12 at $M = 0.2$ and 0.6, with and without a $0.01c$ height Gurney flap positioned at $1.0c$.

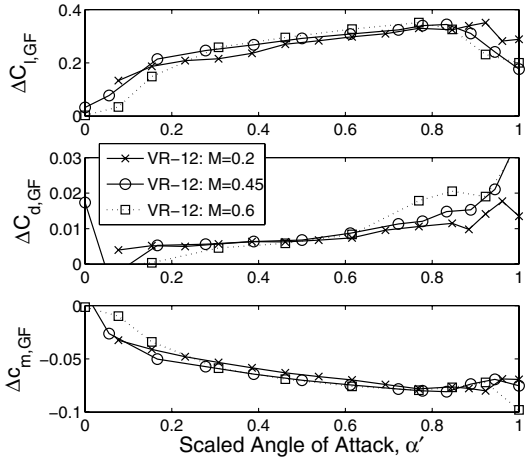

Fig. 9 Computed effects of a Gurney flap with compressible variations: a) lift vs α', b) drag vs α', and c) pitching moment vs α'.

$$\alpha' = \frac{\alpha - \alpha_{n\text{STALL}}}{\alpha_{p\text{STALL}} - \alpha_{n\text{STALL}}} \tag{1}$$

where $\alpha_{n\text{STALL}}$ and $\alpha_{p\text{STALL}}$ are the negative and positive stall angles of attack. As can be observed in Fig. 9, the application of this scaling essentially removes the influence of Mach number on the changes in the force and moment coefficients due to a Gurney flap. As $\alpha' \to 0$, the effects of a Gurney flap approach those of the baseline airfoil as its influence becomes negligible. Thus, the Mach number dependency on the changes in the lift coefficient due to a Gurney flap can be treated as

$$\Delta c_{l,\text{GF}}(M, \alpha) = \Delta c_{l,\text{GF}}(\alpha') \tag{2}$$

Equation (2) suggests a method of accounting for the aerodynamic effects of a Gurney flap on a specific airfoil at different flow conditions without experimentally or computationally determining these effects at each Mach number. In this way, accounting for Gurney-flap aerodynamics through a range of highly variable flow conditions requires only a few experimentally or numerically determined cases. The drag and pitching-moment coefficients can be treated in the same way. In theory this presents a straightforward scaling approach, however, it depends a priori on knowing the stall behavior, which can be difficult to determine both experimentally and computationally.

IV. CFD Validation for Dynamic Conditions

A. Oscillating Airfoil Validation

Using a consistent approach in grid development, models were made to represent an oscillating VR-12 airfoil to validate the results from OVERFLOW2 using measurements made in the Compressible Dynamic Stall Facility at the Nasa Ames Research Center [16,39]. In these experiments, a Gurney-flap-equipped VR-12 airfoil was oscillated through angles of attack from 0 to 20 deg using a sinusoidal oscillation of $\alpha = 10\,\text{deg} + 10\,\text{deg}\sin(\omega t)$. For the cases modeled here, the experimental conditions of $M = 0.4$ and $k = 0.1$ were matched. The experimental setup is only partially represented in these simulations. Here, the measured airfoil coordinates from the VR-12 model are used in the CFD model. However, the CFD uses far-field boundaries positioned $10c$, as compared with the wind-tunnel walls that are less than $1c$, from the unpitched chord line. The CFD and wind-tunnel results for the lift, drag, and pitching-moment coefficients are presented in Fig. 10. It is evident that OVERFLOW2 predicts accurate trends in the aerodynamic behavior, as well as forces and moments, for both the baseline and Gurney-flapped cases. Figure 10 displays moderately large deviations in the predicted aerodynamics, however, although such deviations might be expected as a consequence of the differences between the wall-corrected flow in the wind tunnel and that of the computations. Comparing the CFD prediction of lift to that measured in the wind tunnel, Fig. 10c, the computational predictions have a lower linear-lift-curve slope, stalls at a higher angle of attack, and stalls with a similar lift coefficient. These discrepancies are quite reasonable in that the tunnel wall effects can increase the lift-curve slope without affecting the lift coefficient at stall, a behavior obvious in this comparison. Furthermore, because the experimental results were obtained using pressure integration, they do not account for viscous contributions or pressure drag on the Gurney flap, thus the predicted drag is higher than that measured. Despite these differences, the changes in the aerodynamic quantities due to a Gurney flap are predicted accurately, including the effects on the lift, drag, and pitching-moment coefficients. The reduction in the stall angle of attack is also captured well. Although not presented here, the flowfield predictions show the correct characteristics of an airfoil in dynamic stall. Likewise, the predictions obtained for $M = 0.3$, also not shown but available in [19], are in reasonable agreement with the experimental results [16,39].

B. MITE Deployment Simulations

Although experimental measurements of deploying MITEs on oscillating airfoils are desirable, performing the appropriate

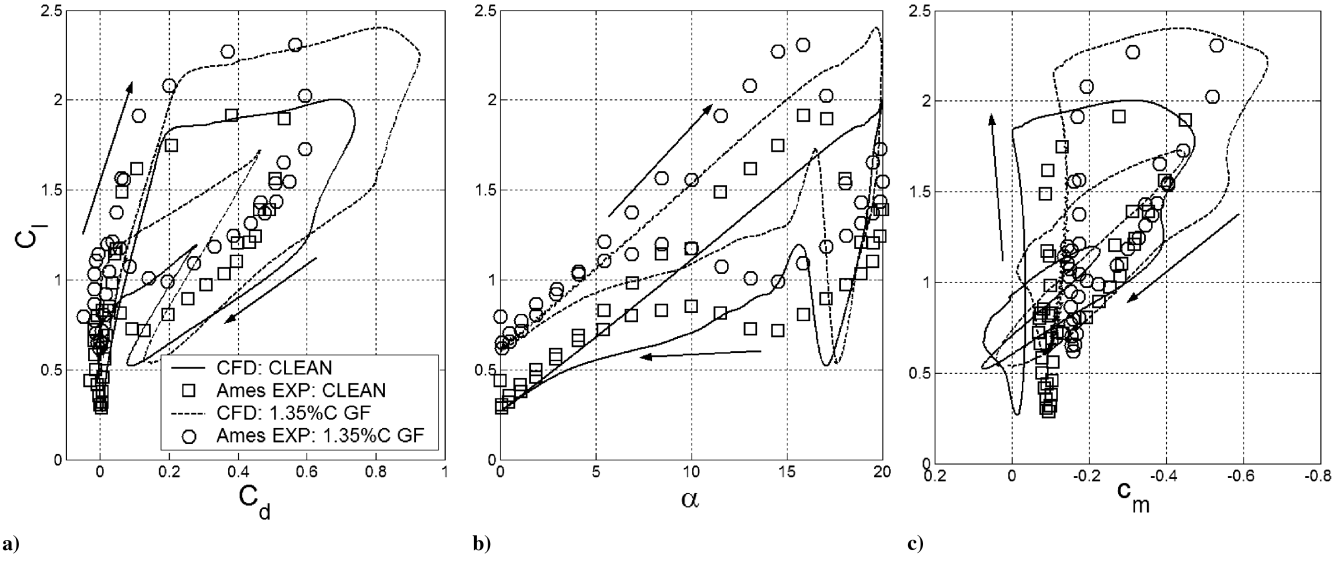

Fig. 10 Aerodynamics predictions of CFD compared with experiment [16,39] through dynamic stall: a) lift vs drag, b) lift vs angle of attack, c) lift vs pitching moment.

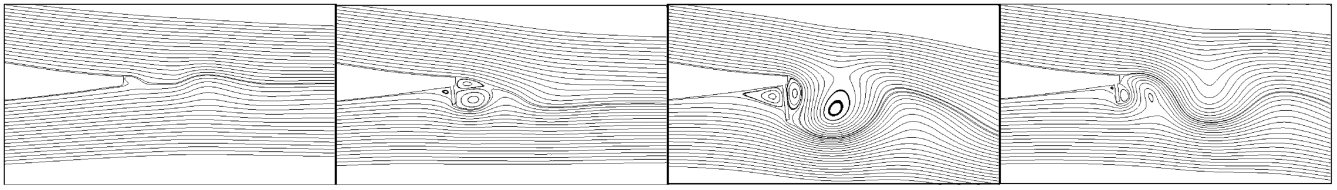

a) δ_{MiTE} = 0.0c b) δ_{MiTE} = 0.01c (deploying) c) δ_{MiTE} = 0.02c d) δ_{MiTE} = 0.01c (retracting)

Fig. 11 Instantaneous streamlines calculated for a 0.02*c* MITE positioned at the airfoil trailing edge.

experiment would be complicated and costly. Therefore, computational methods are well suited for the initial studies. These types of problems are ones for which CFD predictions are ideal for helping to increase the understanding of the physics, before implementation and conducting costly experiments. The following results are intended to explore the aerodynamics of MITEs for rotorcraft purposes, which can provide guidance for future efforts.

For rotorcraft, MITEs show potential for applications requiring two very different frequencies. For vibration control, deployment would occur on the order of 4 deployments per revolution of the rotor, or about 20 Hz, while performance enhancement would require one deployment per revolution, or about 5 Hz. Given that the unsteady effects are most conveniently characterized in terms of reduced frequency, the large radial and azimuthal variations in V that occur on a rotor dictate that MITE performance must be considered over a wide range of reduced frequencies.

The investigations begin with the S903 airfoil, for which static wind-tunnel data is available. The flow conditions for these cases are similar to those of the inner portion of a retreating blade. These cases are intended to give confidence in the modeling strategies, which can then be extended and applied to conditions and airfoils more applicable to rotorcraft. The chordwise positioning of MITEs has also been investigated to provide insight for several different implementation concepts and to better understand the affect of the MITE location.

1. *MITE Positioned at the Airfoil Trailing Edge*

For the first case, the MITE is taken to be at the trailing edge of the S903 airfoil. It is scheduled to have sinusoidal surface-normal deployments at the expected operational frequencies of 5 and 20 Hz, corresponding to the reduced frequencies of $k = 0.14$ and $k = 0.56$, respectively. The flow conditions imposed are similar to those of the low-speed wind-tunnel experiments [2]. Instantaneous streamlines for the 20 Hz case through one cycle are shown in Fig. 11. In the retracted position, the flow is smooth and well behaved. When initially deploying, the amplitudes of the flow oscillations are relatively small, as displayed in Fig. 11b; however, at greater deployment heights, Fig. 11c, larger flow oscillations develop and a vortex street, resembling that observed with the static Gurney-flap simulation, forms. As depicted in Fig. 11d, during the retraction these vortical oscillations have greater amplitudes than when deploying, Fig. 11b. This indicates that the oscillations die out at a lower displacement height than that at which they first occur during deployment. It should be noted that the predicted flow structure closely resembles that found experimentally [23,35]. These flow features are apparent in the lift, drag, and pitching-moment coefficients, as plotted against the MITE deployment height in Fig. 12. During the deployment, the expected lag in lift is apparent in the nonlinear lift response. Furthermore, the previously described flow oscillations arise as high-frequency loading events, which also displays that the retracting MITE possesses flow oscillations at lower deployment heights than does a deploying MITE. Both deployment frequencies are compared against steady-state CFD and experimental predictions of an equivalently sized and positioned Gurney flap. With respect to these steady conditions, the predicted MITE aerodynamics behaves as expected. Compared with the static Gurney flap, the amplitudes decrease with increased frequency, but most important, the devices maintain functionality with high-frequency deployments.

Next, the VR-12 airfoil is considered with a MITE of height of $0.01c$ positioned at the trailing edge. For this case, deployments are made at numerous frequencies and flow conditions. These results are summarized in the reduced frequency domain as shown in Fig. 13.

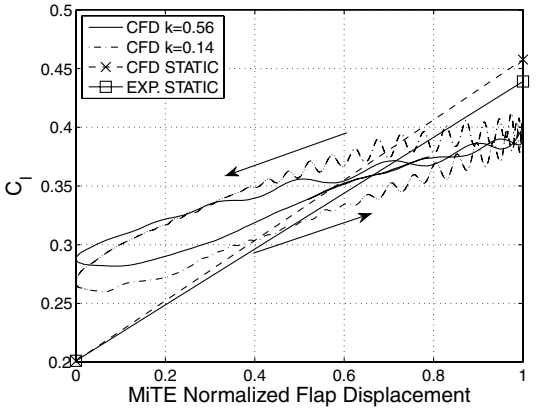

a) Lift

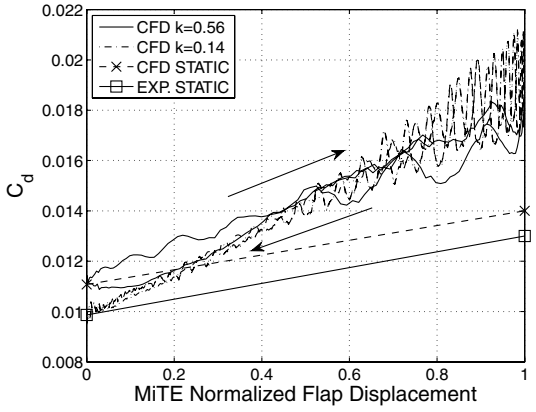

b) Drag

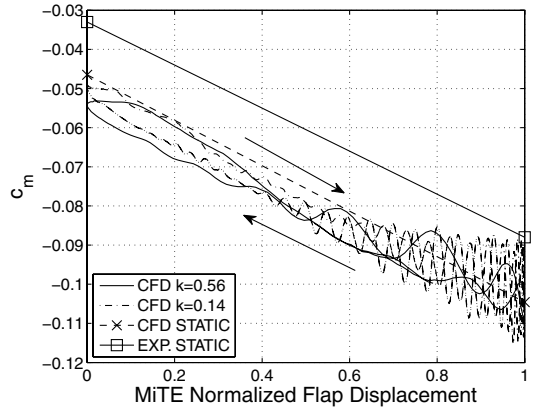

c) Pitching moment

Fig. 12 Predicted aerodynamics for the sinusoidal deployment of a MITE positioned at the trailing edge.

Here, the normalized lift is compared with the circulatory unsteady model, the Theodorsen circulation function [23]. In comparison to the theoretical results, CFD predicts an agreeable trend in amplitude reduction with increased frequency and nearly an identical phase-lag behavior. It should be noted that the amplitude is computed using the mean lift response, i.e., the high frequencies are filtered, and the phase lag is measured by the delay in maximum lift from the maximum MITE deployment height. These results also agree with the CFD simulations of MITEs deploying on both the pressure and suction surfaces, as presented in [8,9,12,13]. As these behaviors agree well with the circulatory-based theory, it is apparent that the circulatory effects dominate the unsteady aerodynamics of MITEs. Furthermore, the underpredicted amplitudes suggest that viscous-driven vortical structures shedding from the deploying MITEs contribute additional vorticity in the wake that contributes to the discrepancies. As deploying MITEs shed vortical structures with a sign equal to circulatory-driven shed vorticity into the wake, the amplitude is expected to decrease while retaining an identical phase lag similar to behavior displayed in the predictions. In general, the strong agreement in trends with theory, along with physically reasonable discrepancies, gives confidence in the validity of these dynamic CFD solutions.

2. *MITE Positioned Upstream of the Airfoil Trailing Edge*

As has been described, the intention of placing MITEs upstream of the trailing edge is to allow them to be stowed within the airfoil. Similar to before, these initial simulations model the MITE on the S903 airfoil using flow conditions similar to those of the wind-tunnel experiments [2]. This case is presented to give confidence in the modeling strategies in that the static wind-tunnel data can be used for validation at the limits of the unsteady cases. As before, the MITEs are deployed at 5 and 20 Hz, corresponding to reduced frequencies of $k = 0.14$ and 0.56, respectively. The instantaneous streamlines for the 5 Hz case through a complete deployment cycle are shown in Fig. 14. It should be noted that in the retracted position, the flow near the MITE is unchanged from what occurs on the airfoil without a MITE. This is not the case when the deployment frequency is increased, in which case visualizations show that the flow is unattached downstream of the MITE and is never able to reestablish to the fully attached situation. As the MITE deploys, a strong vortex forms downstream of the MITE and advects to the trailing edge of the airfoil. The time required for this is a significant portion of the deployment cycle, especially for the 20 Hz case. Then, as the MITE retracts, a weaker vortex remains and spans from the MITE to the trailing edge of the airfoil, finally shedding after the MITE fully retracts. As shown in Fig. 15, where the predicted aerodynamic responses are plotted at the two deployment frequencies, the aerodynamic coefficients are significantly influenced by the presence of this vortex. It is noted that the maximum lift is not achieved until the vortex reaches the trailing edge. This is a result of the strong vortex that develops as the MITE deploys, which is pictured in Fig. 14b. This vortex creates a low-pressure region on the lower surface of the airfoil that counters the production of lift. This is similar, but in an opposite sense, to the vortex lift observed in dynamic stall. In addition, flow visualizations show that when the vortex reaches the trailing edge, the low-pressure core entrains air from the suction surface and creates additional circulation over the entire airfoil. This entrained air balances the pressure and reduces the vortex strength, enabling the maximum lift to finally be achieved. These combined effects are responsible for the sharp lift increases generated. The drag is slightly increased in the low-frequency case, where the flow has the time to reattach. For the high-frequency case, where the time required for the vortex to reach the trailing edge approaches that of the deployment cycle, the flow does not have time to reattach and the drag is increased significantly.

The effects of the chordwise MITE location are further assessed in a summary of the results presented in Fig. 16. These predictions were generated for the VR-12 airfoil having a MITE of height $0.02c$ positioned at several chordwise locations. The results are for $R = 1.4 \times 10^6$, $M = 0.4$, and $k = \pi/2$. The presence of the vortex

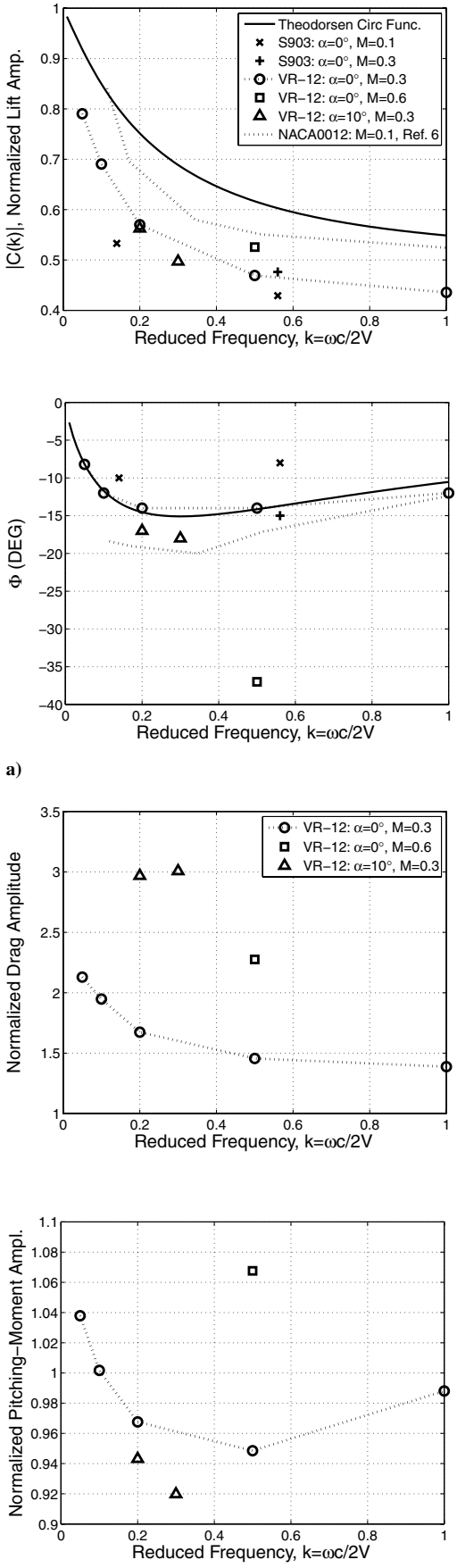

Fig. 13 Computed aerodynamic effects for a MITE positioned at the trailing edge, with changes in deployment frequency, freestream conditions, and compared with incompressible theory [23]: a) lift and phase of lift, and b) drag and pitching moment.

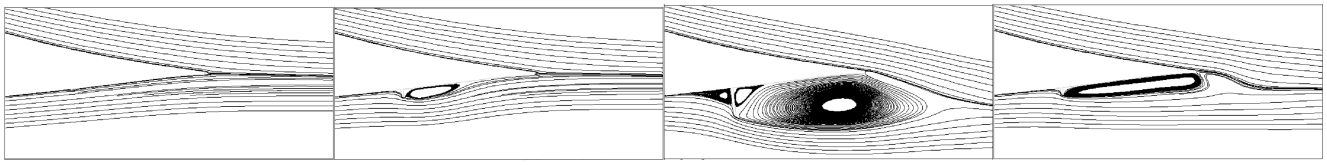

a) δ_{MiTE} = 0.0c b) δ_{MiTE} = 0.01c (deploying) c) δ_{MiTE} = 0.02c d) δ_{MiTE} = 0.01c (retracting)

Fig. 14 Instantaneous streamlines calculated for a $0.02c$ MITE positioned at $x = 0.9c$ and deploying at 5 Hz ($k = 0.14$).

clearly influences the lift, drag, and pitching-moment coefficients, where upstream positioning increases the time required for the vortex to be transported to the trailing edge. In general, increased upstream positioning enlarges the hysteresis loop and degrades the lift enhancement. Also, as expected, the positioning increases the drag and decreases the nose-down pitching moment.

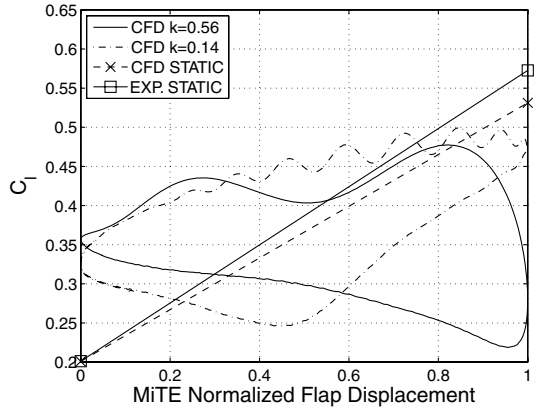

a) Lift

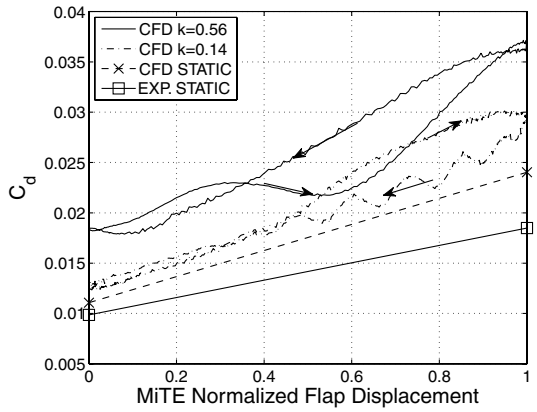

b) Drag

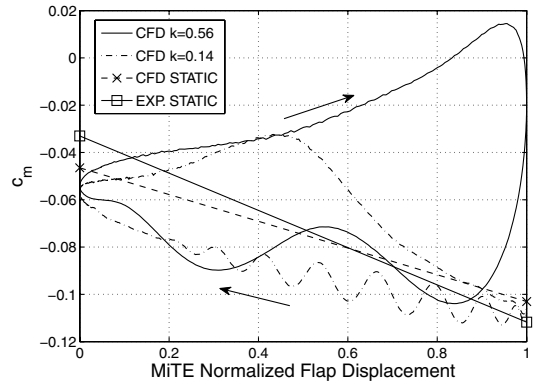

c) Pitching moment

Fig. 15 Predicted aerodynamics for the sinusoidal deployment of a MITE located at $0.9c$.

Next, the VR-12 airfoil is modeled with a MITE height of $0.02c$ and positioned at $0.9c$. Simulations having sinusoidal deployments at numerous frequencies and flow conditions were calculated, the results of which are summarized in the reduced frequency domain and presented in Figs. 17–19. The normalized lift and phase angles are presented for comparison to Theodorsen's circulation function [23] in Fig. 17, and it is noted that the predicted lift amplitudes are greater than those of the theory. This disagreement, however, does not invalidate the CFD results, because among the assumptions used in developing the theory are those clearly unsatisfied by a deploying MITE that limit the application to small disturbances and fully attached, inviscid flows. The flow around an upstream MITE, which is characterized by a large, unattached vortex that develops with deployment and advects downstream, is not taken into account by the Theodorsen function, nor can the computational results be fully validated by results obtained for conventional flaps. The predicted flowfield features for this upstream MITE configuration, including

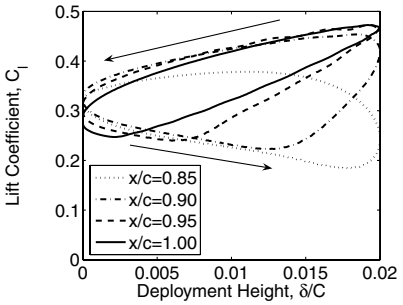

a) Lift

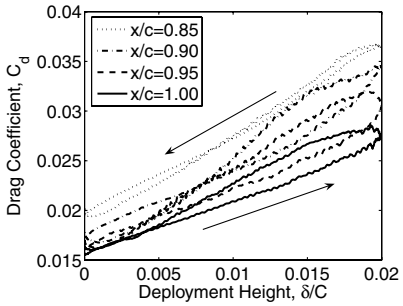

b) Drag

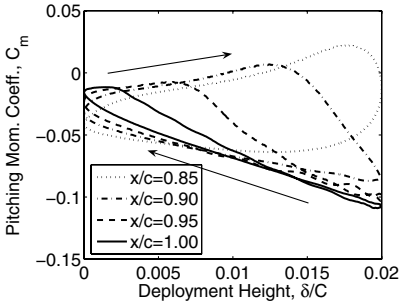

c) Pitching moment

Fig. 16 Predicted aerodynamics for the sinusoidal deployment of a MITE located at various chordwise locations on the VR-12 airfoil.

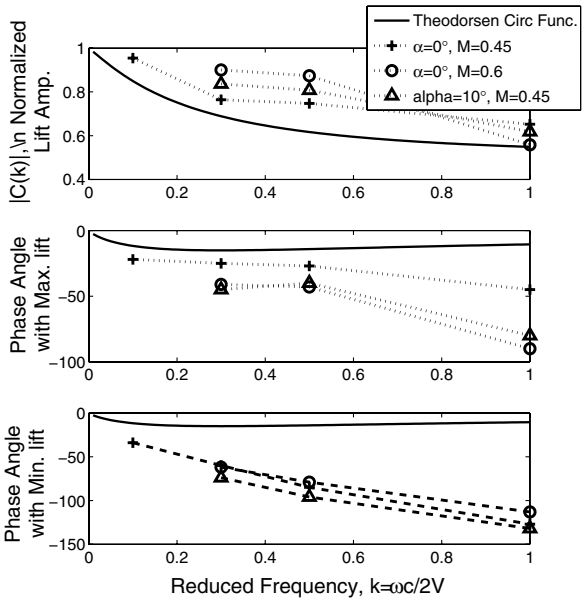

Fig. 17 Effect of the lift with changes in deployment frequency of a MITE positioned at 0.9*c* for various freestream conditions and compared with incompressible theory [23].

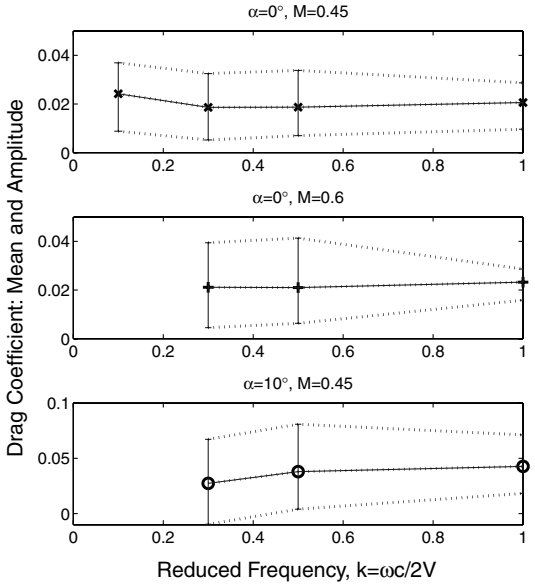

Fig. 18 Effect of drag for a MITE positioned at 0.9*c* at various deployment frequencies and freestream conditions. The upper, middle, and lower lines indicate the maximum, mean, and minimum drag, respectively, through the deployment cycle.

the vortex that forms behind the MITE during deployment and its advection downstream along the lower surface, produces a very different flow than does a trailing-edge MITE or a conventional flap. As a consequence, the phase lags between full deployment and maximum lift generation are very different from those occurring between fully retracted and minimum lift. For this reason, they are plotted separately in Fig. 17. Because of the influence of the vortex that forms behind the flap, as the deployment frequency increases the lag in lift development is increasingly unlike that predicted by the Theodorsen function for a conventional trailing-edge flap. Finally, as a consequence of the vortex system reducing the lift as the MITE deploys, it should be noted that the phase lag at the minimum lift position is much larger than that at the maximum lift.

The predicted drag coefficients in the reduced frequency domain for different Mach numbers are presented in Fig. 18. Here, the expected increase in mean drag with increasing deployment frequency is not observed as it was for the S903 airfoil. For these cases, however, the Mach and Reynolds numbers are significantly higher than those used in the S903 airfoil computations. These differences appear to allow the flow to reattach at increased frequencies, such that the drag increases at higher deployment frequencies are not observed through the range of calculations. This is promising for high-frequency applications, where at higher Mach and Reynolds numbers significant drag increases are not apparent, extending the practical limits of an upstream MITE concept. An interesting case is simulated at an angle of attack of 10 deg, which happened to be between the stall angles of attack of the baseline and the Gurney-flap-equipped airfoil. This is representative of a type of dynamic stall occurring on a static airfoil and accounts for the large drag values. The pitching-moment coefficients for these cases are presented in Fig. 19, where the predicted values seem to have little dependence on the deployment frequency.

A MITE placed upstream of the trailing edge still provides increased lift and moment amplitudes, but these gains are accompanied by large increases in the phase lags, added complexities in force responses and, at higher deployment frequencies for low Reynolds numbers, an increase in the predicted mean drag coefficient. In addition, as a consequence of the vortex advection time being fixed by the freestream velocity, changes in the MITE deployment frequency can have a large effect on the predicted aerodynamics.

Lack of experimental or physically derived theoretical models makes it difficult to assess the validity of these predictions. Nevertheless, confidence in these results can be based on the following arguments: 1) the Gurney-flap aerodynamics were captured well, 2) the results are consistent with those of the Theodorsen theory for the trailing-edge MITEs, 3) numerical verification that the solutions are well resolved in time and space, and 4) physically reasonable solutions based on vortical structures forming about a sharp separation point that affects the aerodynamics in a manner similar to the well-documented dynamic-stall phenomena. This logic strongly implies that these CFD simulations are, in fact, reasonable. However, the authors admit that one primary feature that may affect these evaluations is predicting the correct vortex strength using a two-dimensional CFD approach. As these are strong, spanwise-generated vortices that are not expected to break down immediately, the two-dimensional models should remain sufficient to evaluate upstream MITE aerodynamics. The deficiency is that these predictions are based on solutions having a less dissipative vortex than expected in operation and three-dimensional implementations may affect this vortex behavior.

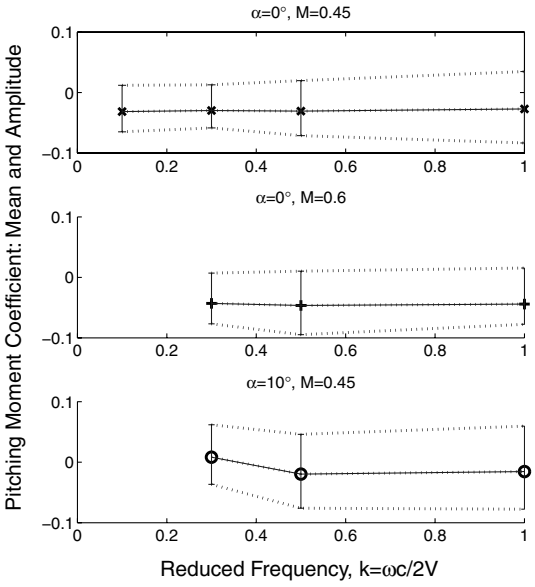

Fig. 19 Effect of pitching moment for MITE located at 0.9*c* at various deployment frequencies and freestream conditions. The upper, middle, and lower lines indicate the maximum, mean, and minimum pitching moment, respectively, through the deployment cycle.

V. Rotorcraft Applications

One anticipated application of MITEs is to increase the lift on the retreating side of the rotor disk and thereby alleviate the effects of blade stall. To explore this more fully and gain insight into an operational situation similar to when a MITE deploys to increase $c_{l,\max}$ on an oscillating airfoil, computational results are presented for a MITE that is deployed on an airfoil in the middle of a pitch oscillation up through dynamic stall. For these simulations, a MITE is positioned at the trailing edge of the VR-12 airfoil operating at $M = 0.4$. MITE deployment is scheduled at an angle of attack where the Gurney-flapped configuration has a higher lift-to-drag ratio than does the baseline; otherwise the MITE is stowed. To demonstrate the unsteady aerodynamics associated with a MITE deployment and how it can be used for dynamic-stall delay, the predicted forces and moments through the deployment are displayed along with the baseline results in Fig. 20. In this case, the MITE is deployed as the airfoil pitches through 10.0 deg. As can be observed in Fig. 20b, after the MITE deploys the lift gradually increases, approaching that of the similarly sized Gurney flap. These results are promising in that the $c_{l,\max}$ obtained with a MITE is comparable to that achieved with a Gurney flap. The drag is presented in Fig. 20a. It is observed that immediately after the deployment, the drag increases and the sectional performance gains are not achieved until the baseline airfoil stalls. It is expected that this drag increase is somewhat exaggerated, as the MITE is modeled to have a rapid deployment, creating additional drag by impulsively blocking the flow. For a more gradual deployment, the increase in drag is expected to be less. In Fig. 20c, the pitching moment is plotted against the angle of attack. As can be observed, the moment remains highly responsive to the MITE position. Finally, it is seen that the MITE continues to be effective poststall. This could be important if MITEs have the possibility of being used for vibration reduction at high speeds, in that their benefit is not limited to nonstalled regions of the rotor disk.

A dynamic-stall control case using a MITE positioned upstream of the trailing edge, at $x/c = 0.9$, is presented in Fig. 21. The MITE is $0.02c$ in height and sized to provide roughly the same increment in $c_{l,\max}$ as does a Gurney flap of $0.0135c$ in height placed at the trailing edge [2]. As displayed in Fig. 21b, the lift initially drops following the MITE deployment, which is expected based on the static airfoil results, but ultimately achieves the same $c_{l,\max}$ as expected for the static Gurney-flap case. The upstream MITE placement also appears to create a case where the flow has difficulty reattaching, which occurs at an angle of attack significantly less than that at which it initially stalls. It should be noted that it is the case that two-dimensional simulations with extensive amounts of separated flow are unreliable, and that this predicted behavior is somewhat suspect. The drag and pitching moments behave as expected and, although a larger increase in drag is predicted initially, it quickly decreases as the vortex advects past the airfoil trailing edge.

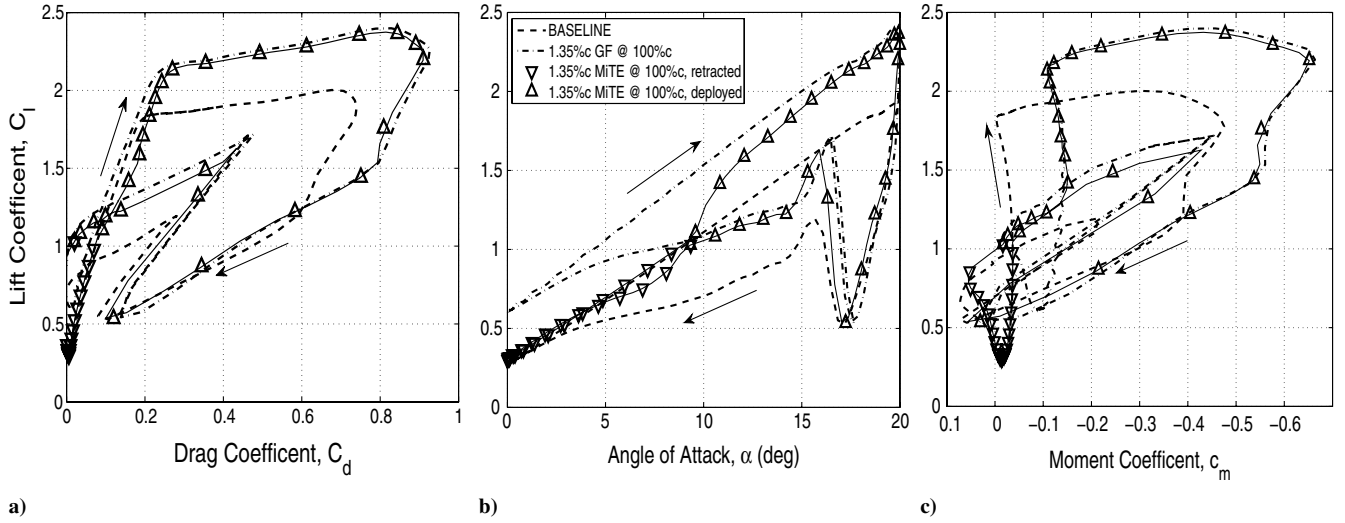

Fig. 20 Force and pitching-moment calculations in dynamic stall for a MITE positioned at the trailing edge: a) lift vs drag, b) lift vs angle of attack, and c) lift vs drag.

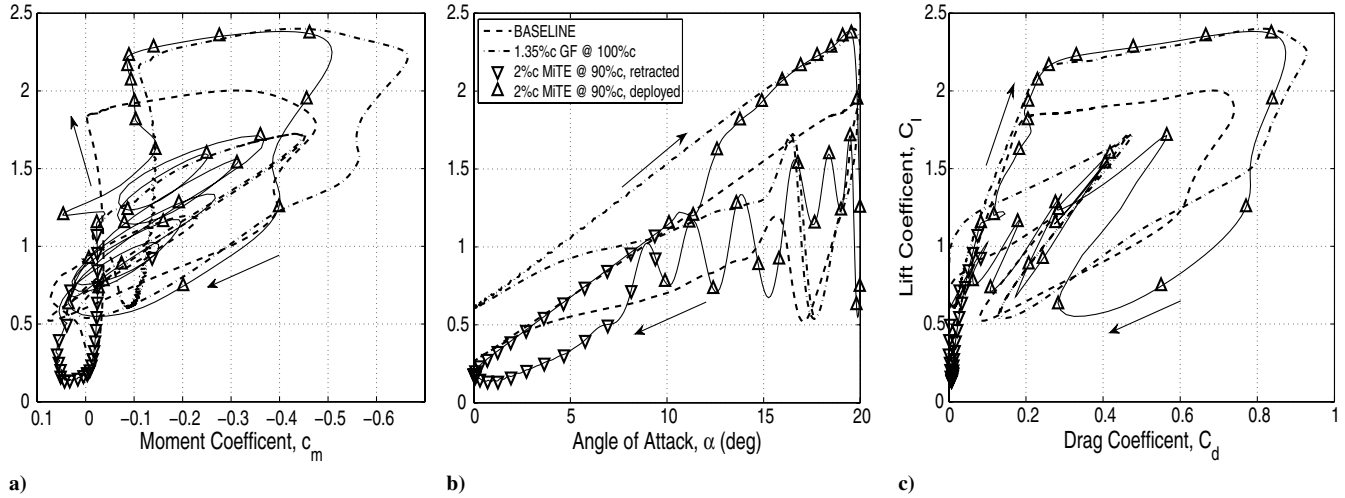

Fig. 21 Force and pitching-moment calculations in dynamic stall for a MITE positioned at $x/c = 0.9$: a) lift vs drag, b) lift vs angle of attack, and c) lift vs drag.

VI. Conclusions

The aerodynamics of MITEs were investigated using CFD to explore their use for improving helicopter performance, as well as for their potential to control vibrations. Of importance in this regard, it is predicted that their performance is not strongly affected by increasing Mach numbers. The studies reported herein addressed MITEs positioned at both the trailing edge of an airfoil and at an upstream location of $0.9c$. The investigations demonstrate that the chordwise location of a MITE greatly affects the unsteady aerodynamics resulting from deployment. When MITEs are positioned at the trailing edge, they appear to remain effective through high deployment frequencies. As they are moved upstream, however, they create strong vortices that propagate downstream along the pressure surface of the airfoil. These vortices delay the development of lift and create a large phase lag between MITE deployment and the resulting aerodynamic forces and moments. This shows that decreases in the sectional performance are possible with high deployment frequencies, which might be a consequence at the low Reynolds number used for the S903 airfoil tests. Finally, it is found that MITEs at any of the chordwise locations explored can sufficiently delay stall. These same MITEs continue to provide lift and moment increments poststall, which may be desirable for vibration control at high speeds.

Acknowledgments

The authors thank the National Rotorcraft Technology Center for the funding of this research. The efforts of P. Martin, C. Tung, M. S. Chandrasekhara of the U.S. Army Aeroflightdynamics Directorate at the Nasa Ames Research Center, and others for providing dynamic experimental data used for these studies, are acknowledged. Likewise, gratitude is given to the developers of OVERFLOW, for providing the computational fluid dynamics code used for this research. S. Allmaras and J. Vassberg of the Boeing Company, and J. Lindau of the Pennsylvania State Applied Research Laboratory are also thanked for their suggestions and insights. Finally, the Pennsylvania State Rotorcraft Center of Excellence is thanked for the many resources used throughout this research.

References

[1] Liebeck, R. H., "Design of Subsonic Airfoils for High Lift," *Journal of Aircraft*, Vol. 15, No. 9, 1978, pp. 547–561. doi:10.2514/3.58406

[2] Maughmer, M. D., and Bramesfeld, G., "Experimental Investigation of Gurney Flaps," *Journal of Aircraft*, Vol. 45, No. 6, Nov.–Dec., 2008, pp. 2062–2067. doi:10.2514/1.37050

[3] Giguére, P., Lemay, J., and Dumas, G., "Gurney Flap Effects and Scaling for Low-Speed Airfoils," *AIAA Applied Aerodynamics Conference*, AIAA Paper 95-1881, 1995.

[4] Baker, J. P., Standish, K. J., and Van Dam, C. P., "Two-Dimensional Wind Tunnel and Computational Investigation of a Microtab Modified S809 Airfoil," *43rd Aerospace Sciences Meeting and Exhibit*, AIAA Paper 2005-1186, 2005.

[5] Kroo, I. M., "Aerodynamic Concepts for Future Aircraft," *AIAA Applied Aerodynamics Conference*, AIAA Paper 99-3524, 1999.

[6] Bieniawski, S., and Kroo, I. M., "Flutter Suppression Using Micro-Trailing Edge Effectors," *43th AIAA/ASME/ASCE/AHS/ASC Structural Dynamics and Mechanics Conference*, AIAA Paper 2003-1941, 2003.

[7] Lee, H., Kroo, I. M., and Bieniawski, S., "Flutter Suppression for High Aspect Ratio Flexible Wings Using Microflaps," *44th AIAA/ASME/ASCE/AHS/ASC Structures, Structural Dynamics, and Materials Conference*, AIAA Paper 2002-1717, 2003.

[8] Lee, H., and Kroo, I. M., "Computational Investigation of Airfoils with Miniature Trailing-Edge Control Surfaces," *2nd AIAA Flow Control Conference*, AIAA Paper 2004-1051, 2004.

[9] Lee, H. -T., "Computational Investigation of Miniature Trailing Edge Effectors," Ph.D. Dissertation, Department of Aeronautics and Astronautics, Stanford Univ., Palo Alto, CA, 2006.

[10] Yen-Nakafuji, D. T., van Dam, C. P., Smith, R. L., and Collins, S. D., "Active Load Control for Airfoils Using Microtabs," *Journal of Solar Energy Engineering*, Vol. 123, No. 4, 2001, pp. 282–289. doi:10.1115/1.1410110

[11] Yen-Nakafuji, D. T., van Dam, C. P., Michel, J., and Morrison, P., "Load Control for Turbine Blades: A Non-Traditional Microtab Approach," *ASME Wind Energy Symposium*, AIAA Paper 2002-0054, 2002.

[12] Chow, R., and van Dam, C. P., "Unsteady Computational Investigation of Deploying Load Control Microtabs," *44th Aerospace Sciences Meeting and Exhibit*, AIAA Paper 2006-1063, 2006.

[13] van Dam, C. P., Chow, R., Zayas, J. R., and Berg, D. E., "Computational Investigations of Small Deploying Tabs and Flaps for Aerodynamic Load Control," The Science of Making Torque from Wind, *Journal of Physics*: Conference Series 75 (2007), 102027, 2007. doi:10.1088/1742-6596/75/1/012027

[14] Kentfield, J. A. C., "The Potential of Gurney Flaps for Improving the Aerodynamic Performance of Helicopter Rotors," *AIAA International Powered Lift Conference*, AIAA Paper 93-4883, 1993, pp. 283–292.

[15] Yee, K., Joo, W., and Lee, D. -H., "Aerodynamic Performance Analysis of a Gurney Flap for Rotorcraft Applications," *Journal of Aircraft*, Vol. 44, No. 3, May–June, 2007, pp. 1003–1014. doi:10.2514/1.26868

[16] Chandrasekhara, M. S., Martin, P. B., and Tung, C., "Compressible Dynamic Stall Performance of a Variable Droop Leading Edge Airfoil with a Gurney Flap," *22nd Applied Aerodynamics Conference and Exhibit*, AIAA Paper 2004-0041, 2004.

[17] Guzel, G., Sankar, L. N., and Rhee, M., "Computational Investigation of the Effects of Gurney Flap on the Aerodynamic Performance of VR-12 Airfoil," *23rd AIAA Applied Aerodynamics Conference*, AIAA Paper 2005-4960, 2005.

[18] Maughmer, M., Lesieutre, G., Thepvongs, S., Anderson, W., and Kinzel, M., "Miniature Trailing-Edge Effectors for Rotorcraft Applications," *American Helicopter Society 59th Forum and Technology Display*, Phoenix, AZ, 2003.

[19] Kinzel, M. P., "Miniature Trailing-Edge Effectors for Rotorcraft Applications," M. S. Thesis, Department of Aerospace Engineering, The Pennsylvania State Univ., University Park, PA, Aug. 2004.

[20] Kinzel, M. P., Maughmer, M. D., Lesieutre, G. L., and Duque, E. P. N., "Numerical Investigation of Miniature Trailing-Edge Effectors on Static and Oscillating Airfoils," *AIAA Aerospace Sciences Meeting*, AIAA Paper 2005-1039, 2005.

[21] Kinzel, M. P., Maughmer, M., and Lesieutre, G., "Miniature Trailing-Edge Effectors for Rotorcraft Performance Enhancement," *Journal of the American Helicopter Society*, Vol. 52, No. 2, April, 2007, pp. 146–158. doi:10.4050/JAHS.52.146

[22] Roedts, R., "Rotorcraft Performance Enhancements Due to a Lower-Surface Effector," M. S. Thesis, Department of Aerospace Engineering, The Pennsylvania State Univ., University Park, PA, Aug. 2008.

[23] Theodorsen, T., "General Theory of Aerodynamic Instability and the Mechanism of Flutter," NACA Rept. No. 496, 1935.

[24] Solovitz, S. A., and Eaton, J. K., "Spanwise Response Variation for Partial-Span Gurney-Type Flaps," *AIAA Journal*, Vol. 42, No. 8, Aug. 2004, pp. 1640–1643. doi:10.2514/1.770

[25] Tang, D., and Dowell, E. H., "Aerodynamic Flow Control of an Airfoil with Small Trailing-Edge Strips," *Journal of Aircraft*, Vol. 43, No. 6, Nov.–Dec. 2006. doi:10.2514/1.18969

[26] Hariharan, N., and Leishman, J. G., "Unsteady Aerodynamics of a Flapped Airfoil in Subsonic Flow by Indicial Concepts," *Journal of Aircraft*, Vol. 33, No. 5, Sept.–Oct. 1996, pp. 855–868. doi:10.2514/3.47028

[27] Buning, P. G., Jespersen, D. C., Pulliam, T. H., Chan, W. M., Slotnick, J. P., Krist, S. E., and Renzeand, K. J., "OVERFLOW User's Manual, Version 1.8," NASA Langley Research Center, Hampton, VA, 1998.

[28] Meakin, B., and Potsdam, M., "Reference Guide for Scalable OVERLOW-D, v1.5e," NASA Ames Research Center, Moffet Field, CA, 2002.

[29] Drela, M., "A User's Guide to MSES 2.95," Massachusetts Inst. of Technology, Cambridge, MA, 1996.

[30] Drela, M., and Youngren, H., "XFOIL 6.94 User Guide," Massachusetts Inst. of Technology, Cambridge, MA, 2001.

[31] Spalart, P. R., and Allmaras, S. R., "A One-Equation Turbulence Model for Aerodynamic Flows," *AIAA 29th Aerospace Sciences Meeting*, AIAA Paper 92-0439, 1992.

[32] Chan, W. M., Rogers, S. E., Nash, S. M., Buning, P. G., and Meakin, R. L., "User's Manual for Chimera Grid Tools", Version 1.6," NASA Ames Research Center, 2001.

[33] Chan, W. M., Gomez, R. J., III, Rogers, S. E., and Buning, P. G., "Best Practices in Overset Grid Generation," *32nd AIAA Fluid Dynamics Meeting*, AIAA Paper 2002-3191, 2002.

[34] Jeffrey, D., Zhang, X., and Hurst, D. W., "Aerodynamics of Gurney Flaps on a Single-Element High-Lift Wing," *Journal of Aircraft*, Vol. 37, No. 2, 2000, pp. 295–301. doi:10.2514/2.2593

[35] Wang, J. J., Li, Y. C., and Choi, K. -S., "Gurney Flap: Lift Enhancement, Mechanics and Applications," *Progress in Aerospace Sciences*, 44, 2008, pp. 22–47. doi:10.1016/j.paerosci.2007.10.001

[36] Richter, K., and Rosemann, H., "Experimental Investigation of Trailing-Edge Devices at Transonic Speeds," *The Aeronautical Journal*, Vol. 106, No. 1058, April 2002, pp. 185–193.

[37] Standish, K. J., and van Dam, C. P., "Computational Analysis of a Microtab-Based Aerodynamic Load Control System for Rotor Blades," *Journal of the American Helicopter Society*, Vol. 50, July 2005, pp. 249–259. doi:10.4050/1.3092861

[38] Dadone, L. U., "Future Directions in Helicopter Rotor Development," *Proceedings from the American Helicopter Society National Specialists' Meeting on Aerodynamics and Aeroacoustics*, The American Helicopter Society, Alexandria, VA, 1987.

[39] Martin, P. B., McAlister, K. W., Chandrasekhara, M. S., and Geissler, W., "Dynamic Stall Measurements and Computations for a VR-12 Airfoil with Variable Droop Leading Edge," *American Helicopter Society 59th Forum and Technology Display*, The American Helicopter Society, Alexandria, VA, 2003.

F. Coton
Associate Editor